

Longitudinal analysis of Disturbed dynamo magnetic signatures

Castellanos-Velazco C. I.^{1,3} Corona-Romero P.^{2,3} Sergeeva M.^{2,3}

¹Universidad Nacional Autonoma de Mexico, Posgrado en Ciencias de la Tierra

² Laboratorio Nacional de Clima Espacial

³ Instituto de Geofisica

Abstract

The present study seeks to analyze longitudinally, the magnetic fluctuations associated with the disturbed dynamo electric field (DDEF) using 11 observatories encircling the globe at mid-low latitudes. The event to be studied is the geomagnetic storm known as the Saint Patrick event due to his main phase was developing during that celebration (march 17th, 2015). In the present studio, we perform a wavelet spectrum in combination with cross-wavelet technique and a semblance analysis studio in order to isolate the DDEF magnetic signatures.

Keywords: Disturbed dynamo, wavelet

1 Introduction

During geomagnetic storms (GS), one of the responses which arise in the ionosphere is the driving of electric currents. In the case of mid-low geomagnetic latitude ranges, we highlight the presence of the Disturbed dynamo (Ddyn) and the disturbed polar current number 2 (DP2).

1.1 Geomagnetic Data

The geomagnetic data analyzed in this paper corresponded to the observatories shown within the Table 1. Magnetic data was obtained from INTERMAGNET (*International Real-Time Magnetic Observatory Network* [5]) where as it is shown, all the observatories are present within the a narrow range of magnetic latitude ($21 - 33^\circ$). On the other hand, this observatories envelope quite different Universal Time (UT) zones. A limitation for the aim of this project is the lack of availability data from some observatories during the period of interest besides there the absence of points lacking ground based magnetometers due to the geography. In the end it was decided to divide the longitudinal study in five sectors, in function of the UT zones for each observatory:

1. sector 1: GUI (UT 0), TAM (UT 1)
2. sector 2: JAI (UT 5:30)
3. sector 3: LZH, BMT (UT 8), CYG, KNY, KAK (UT 9)
4. sector 4: HON (UT -10)
5. sector 5: TEO (UT -6), SJG (UT -4)

Although the distance between each observatory presents a limitation for analyzing the longitudinal develop of the GS and its regional response, we can still analyze the response within different time sectors in which each observatory was present during the main phase.

Table 1: List of observatories considered for this study.

| Country | Observatory | IAGA code | geographic latitude | geographic longitude | magnetic latitude | magnetic longitude | UT h |
|------------------|-------------|-----------|---------------------|----------------------|-------------------|--------------------|------|
| China | Beijing | BMT | 40.3 N | 116.2 E | 30.53 N | 172 W | 8 |
| South Korea | Cheongyang | CYG | 36.37 N | 126.854 E | 27 N | 162.43 W | 9 |
| India | Jaipur | JAI | 26.917 N | 75.8 E | 18.42 N | 150.47 E | 5.5 |
| Spain | Guimar | GUI | 28.317 N | 16.433 W | 33.21 N | 61.1 E | 0 |
| USA | Honolulu | HON | 21.317 N | 158 W | 21.49 N | 90.03 W | -10 |
| Japan | Kakioka | KAK | 36.232 N | 140.186 E | 27.8 N | 149.73 W | 8 |
| Japan | Kanoya | KNY | 31.417 N | 130.867 W | 22.3 N | 158.4 W | 9 |
| China | Lanzhou | LZH | 36.083 N | 103.833 E | 26.23 N | 176.79 E | 8 |
| USA, Puerto Rico | San Juan | SJG | 18.11 N | 66.15 W | 28.19 N | 6.1 E | -4 |
| Argelia | Tamanraset | TAM | 22.783 N | 5.571 E | 24.3 N | 82.29 E | 1 |
| Mexico | Teoloyucan | TEO | 19.747 N | 99.182 W | 27.81 N | 28.4 W | -6 |

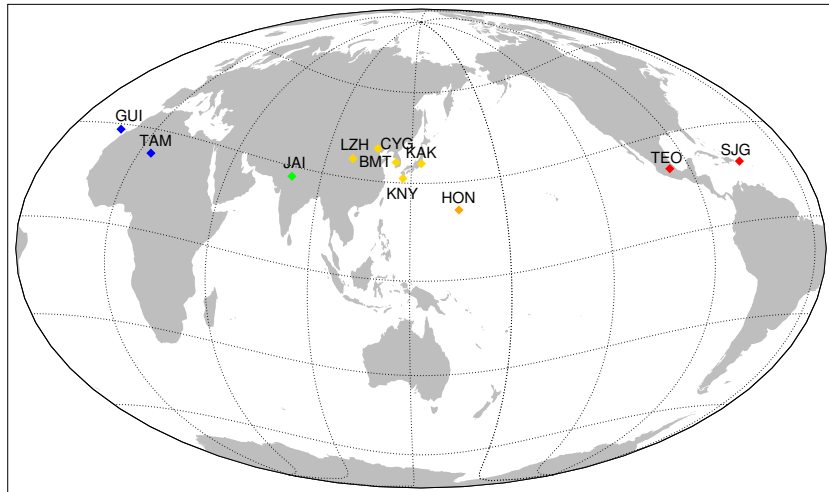


Figure 1: Geographic position of every magnetic observatory considered for this study. The color code corresponds to different local time regions: blue (UT 0, 1), green (UT 5:30), yellow (UT 8, 9), orange (UT -10), red (-6, -4).

2 Methodology

2.1 Isolation of magnetic fluctuations of ionospheric origin

According to [4, 6, 8, 10], we can approach the recordings of a local magnetometer as:

$$H_{loc} = H_{SQ} + H_0 + H_{MT} + H_I, \quad (1)$$

where H_{SQ} is the diurnal variation and H_0 is the monthly baseline, we deepen about how we model them in the Appendix A. H_{MT} on the other hand are the variations induced due to the magnetospheric currents activity and intensification during the GS. Finally, H_I stands for the magnetic variations driven by ionospheric currents activity during a GS.

For mid-low magnetic latitudes, according to [11], we can approach roughly enough H_{MT} as $H_{MT} \approx SYM - H \cdot \cos(\lambda)$, being λ the geomagnetic latitude of each observatory, shown in column 6 of Table 1. Thus H_I can be approached by:

$$H_I = H_{DDEF} + H_{PPEF} \approx H_{loc} - (H_{SQ} + H_0 + SYM - H \cdot \cos(\lambda)) \quad (2)$$

being H_{DDEF} and H_{PPEF} the magnetic field associated with the disturbed dynamo electric fields and the prompt penetration electric fields respectively.

2.2 Time-Frequency Analysis

In order to isolate H_{DDEF} and H_{PPEF} from each other, we can proceed from the consideration that both ionospheric currents induce quasi periodic fluctuations [1, 7, 11]. Hence we begin with a Fourier Analysis, setting passband filters for fluctuations of periods 24 h to reconstruct H_{DDEF} , meanwhile using highpass filters to reconstruct H_{PPEF} .

However, Fourier analysis only give a frequency domain perspective. In order to analyze also the time domain, we perform wavelet techniques [9], as done in [12] in order to compare two time series (H_{SQ} and H_I) which have similar band frequency fluctuations ($f \approx 1.15e - 5Hz$ or $T \approx 24h$). Then identify which signal is more correlated to H_{DDEF} activity.

In the present paper, we performed a wavelet analysis (W), using the Morlet function as the mother wavelet. Hence we computed the wavelet spectrum ($|\psi_0|^2$) in order to observe the power of the signal related to H_I . As second stage of this time-frequency analysis, we computed the cross-wavelet:

$$W_n^{SQ, H_I}(s) = W_n^{H_{SQ}}(s)W_n^{H_I*}(s), \quad (3)$$

being s the scale of the wavelet transform and n the index number of each time series. In the right side of equation 3 $W_n^{H_{SQ}}(s)$ is the wavelet transform applied to the diurnal variation meanwhile $W_n^{H_I*}(s)$ is the conjugate of the wavelet transform applied to H_I . The output of this crosswavelet transform we are interested in, are the resulting amplitude α and the local phase θ . Hence we carry out a semblance analysis described by the following equation:

$$\text{semblance} = \cos^n(\theta) \quad (4)$$

being n an odd integer number greater than 1. We set $n = 9$ as tested in [3]. From semblance we can obtain normalized correlation values ranging between -1 and 1, where the signal closer to -1 is highly correlated to H_I , meanwhile the signal closer to 1 is more correlated to H_{SQ} . Considering that semblance does not give information about the intensity of neither of the implied signals, we can multiply it by the amplitude α and compute H_{DDEF} likewise:

$$H_{DDEF} = \alpha \cdot \text{semblance}; \text{semblance}_i \geq 0. \quad (5)$$

Having the wavelet spectrum $|\psi_0(n)|^2$ which give us the power of the signals and $\alpha \cdot \text{anticorr}(\text{semblance})$ which highlights the signal related to H_{DDEF} , we can observe not only weather H_{DDEF} variations are present during the event but also, their intensity.

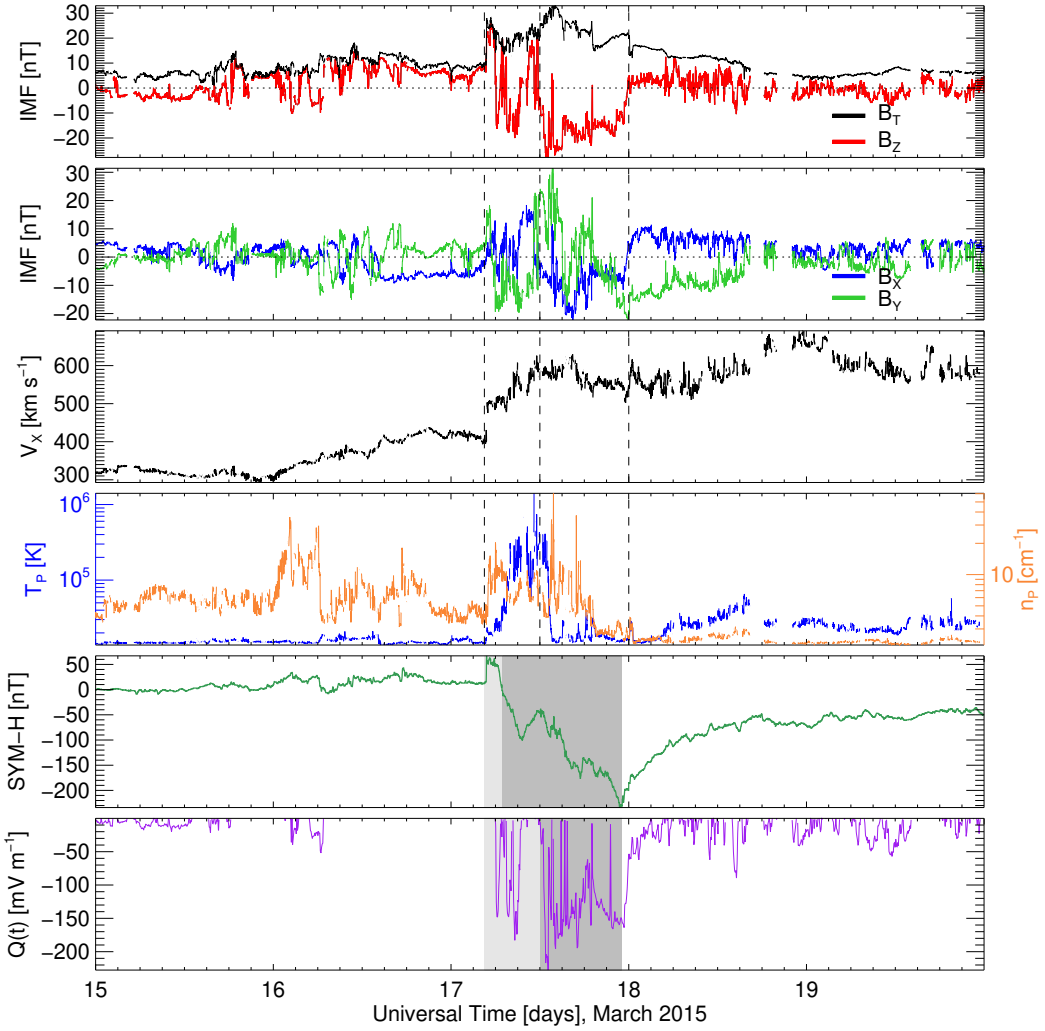


Figure 2: Interplanetary measurements. Panel (a): total interplanetary magnetic field (black line) and z component (red line). Panel (b): V_X component of solar wind velocity (orange line) and proton density (blue line). Panel (c): SYM-H index (green line), highlighting the initial phase (light gray shade), main phase 1 (medium gray shade) and main phase 2 (dark gray shade). Panel (d): Energy input $Q(t)$ (purple line), highlighting with gray and dark gray shade the period of maximum energy input

3 Results

3.1 Interplanetary Studio

3.2 Reconstruction Analysis

3.3 Wavelet Analysis

4 Discussion

5 conclusions

The Ddyn magnetic fluctuations, H_{DDEF} where present in TEO observatory with more intensity since [1]

Another observation found is that TEO is the point at which we observe picks of H_{PPEF} significantly higher than H_{DDEF} fluctuations, but is also the point at which H_{PPEF} gets highest values during this

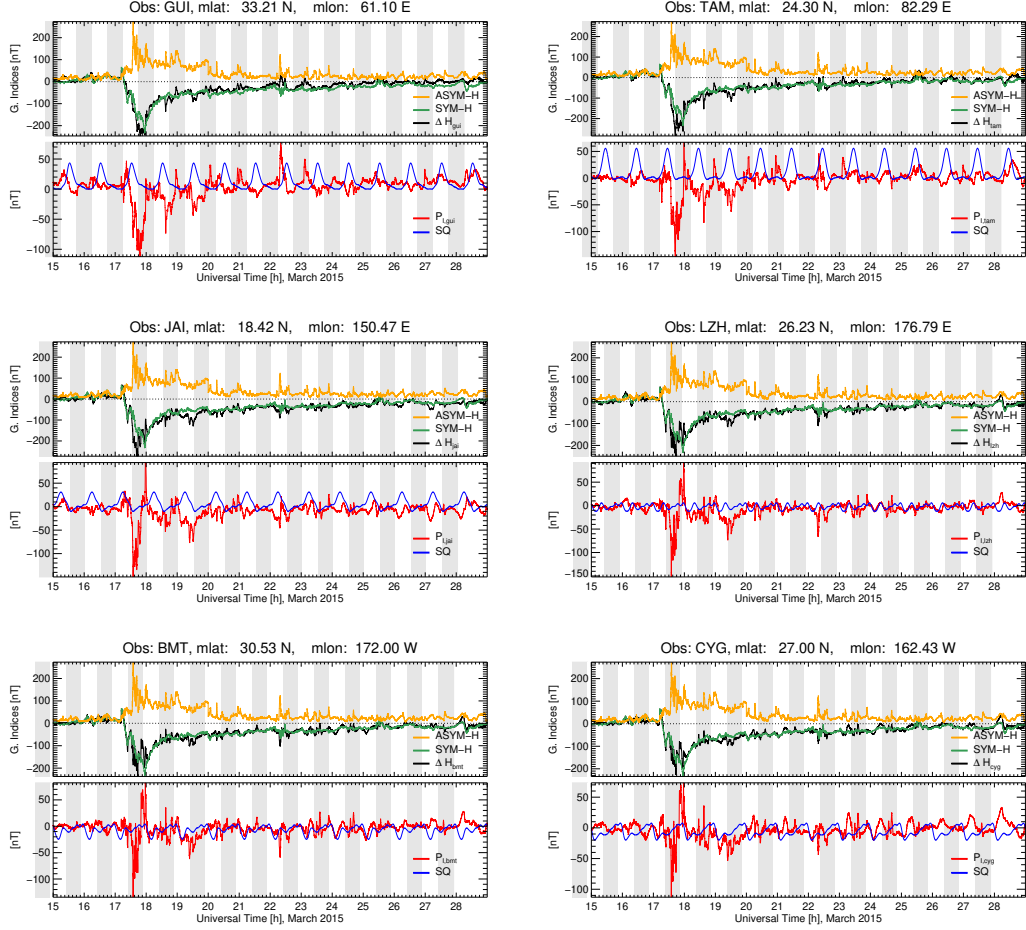


Figure 3: Geomagnetic observations for each magnetic observatory. top panels show planetary geomagnetic indices SYM-H (green line) and local processed magnetic registers (black line). Bottom panels: Magnetic contribution of ionospheric origin (red line) and diurnal variation modeled from local quiet days (blue line) (Part 1)

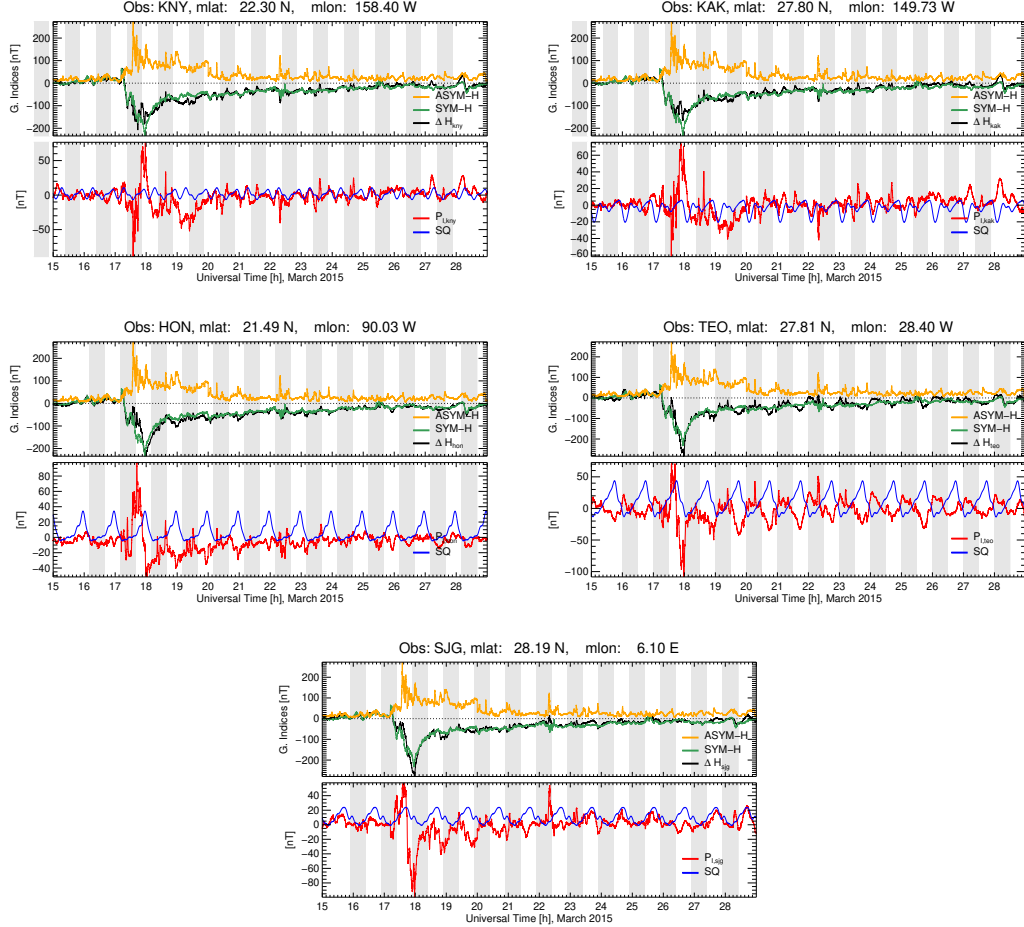


Figure 3: Geomagnetic observations for each magnetic observatory. top panels show planetary geomagnetic indices SYM-H (green line) and local processed magnetic registers (black line). Bottom panels: Magnetic contribution of ionospheric origin (red line) and diurnal variation modeled from local quiet days (blue line) (Part 2)

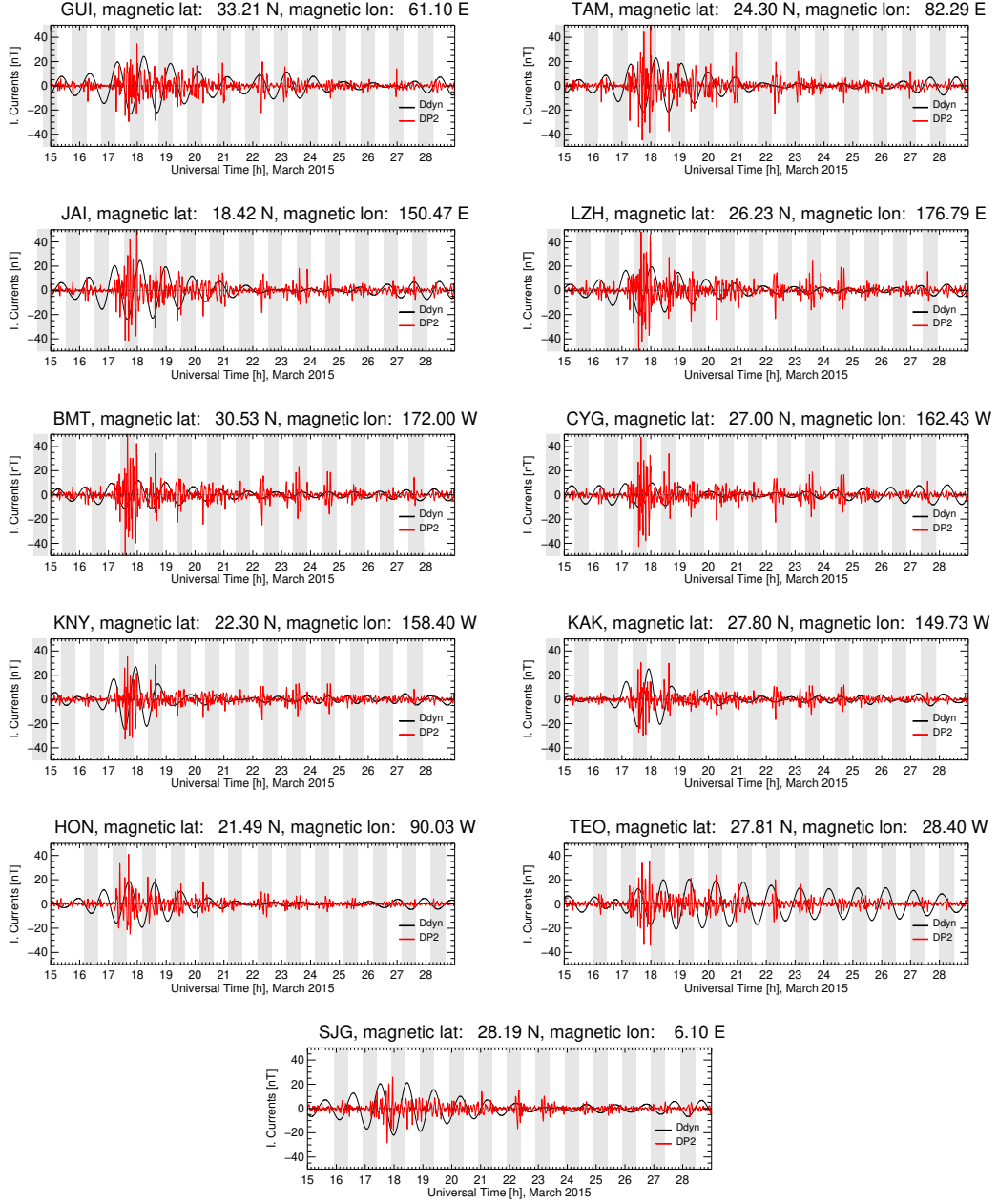


Figure 4: Geomagnetic observations for each magnetic observatory. top panels show planetary geomagnetic indices SYM-H (green line) and local processed magnetic registers (black line). Bottom panels: Magnetic contribution of ionospheric origin (red line) and diurnal variation modeled from local quiet days (blue line) (Part 2)

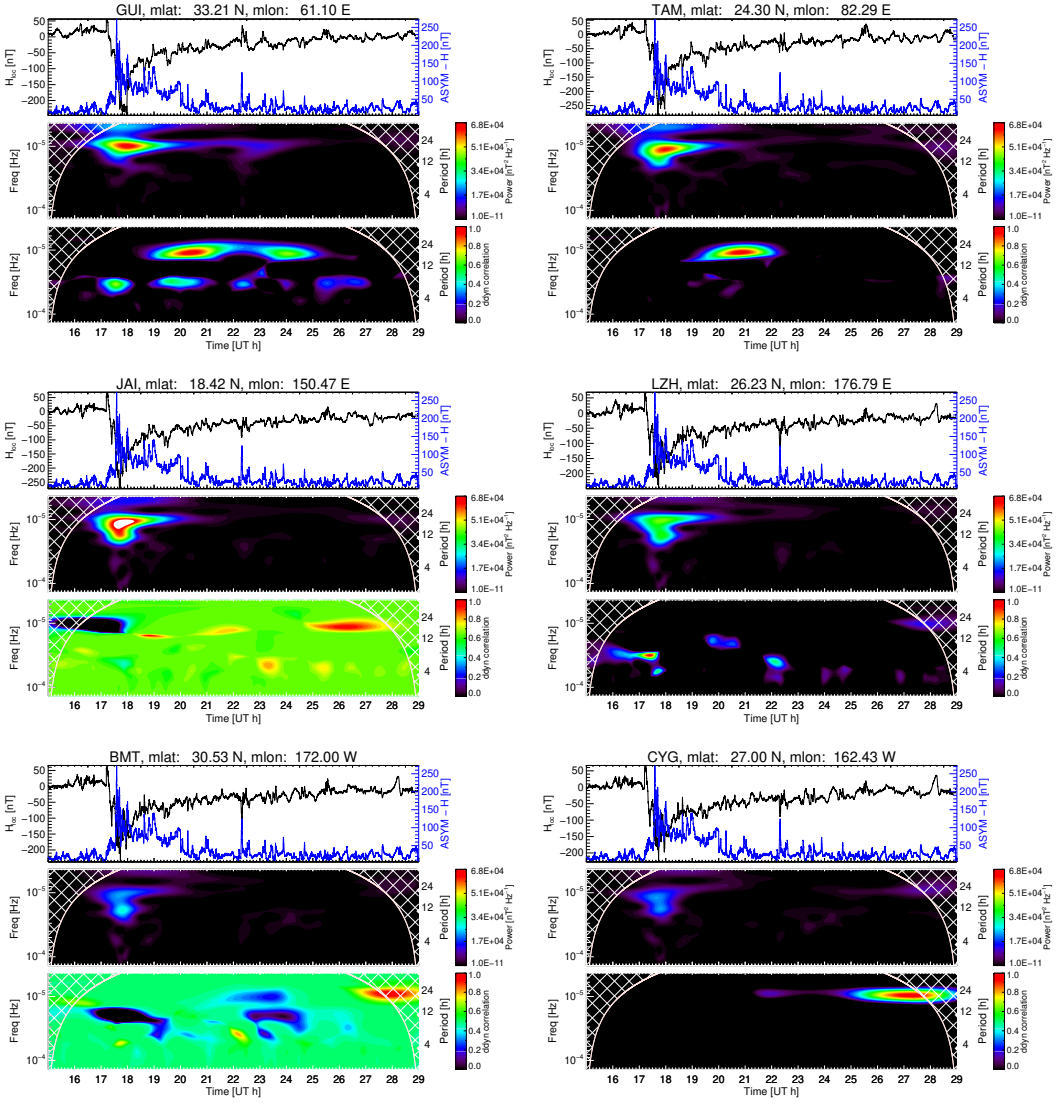


Figure 5: Wavelet Analysis. Top panels: Local H_x magnetic component describing the development of the GS (black line) and ASYM-H index describing asymmetric ring current activity (blue line). Middle panels: wavelet spectrum applied to H_I describing the strength of the ionospheric magnetic contribution signal obtained from $|\psi(n)|^2$. Bottom panels: Ddyn correlation obtained from Eq 5 (Part 1)

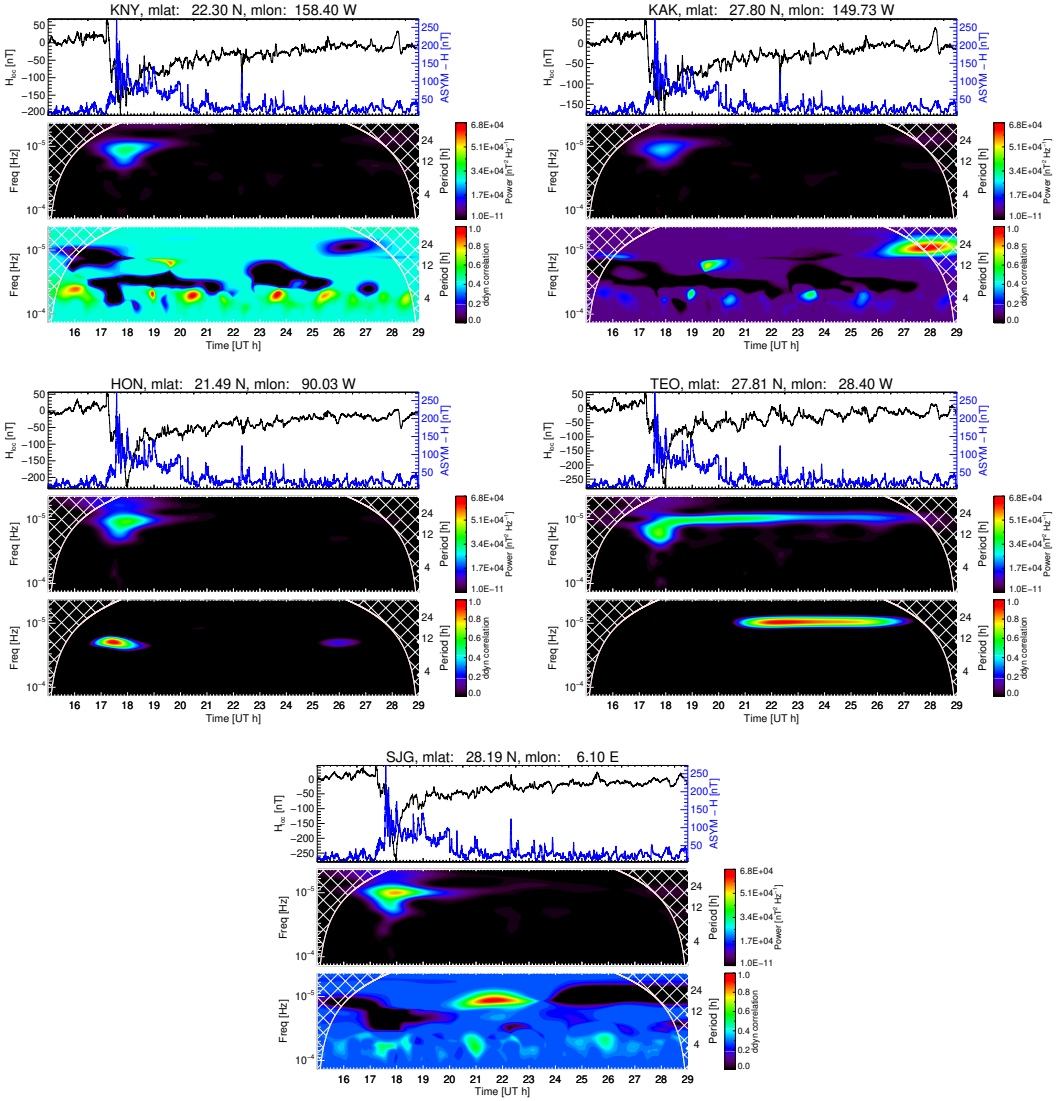


Figure 5: Wavelet Analysis. Top panels: Local H magnetic component describing the development of the GS (black line) and ASYM- H index describing asymmetric ring current activity (blue line). Middle panels: wavelet spectrum applied to H_I describing the strength of the ionospheric magnetic contribution signal obtained from $|\psi(n)|^2$. Bottom panels: Ddyn correlation obtained from Eq 5 (Part 2)

study,

On the other hand, in the results obtained through analyzing magnetic data from observatories within sector 3 which corresponds to LZH, BMT, CYG, KNY and KAK we observe very weak and even null H_{DDEF} . This is consistent with [...].

A Processing magnetic data

It is important to remove the regular variations present within each magnetic register in order to preserve only the magnetic contributions in which we are interested. The main field H_0 which can be removed through modeling a daily monthly baseline, was approximated by computing either the daily mode or a center of a gaussian fit [4] for the local-night magnetic data $H[0 : 3](t)$. Then, we compute H_0 from the median of each daily value in march. To not consider daily values during disturbed days, we filtered them by adapting the procedure in [10]. Hence, we swift a moving window, computing an hourly the Inter Quantil Range (IQR). To filter the disturbed days, we have to set a threshold of variation, where:

$$IQR_{med}^i > \text{threshold} = \text{disturbed} \quad (6)$$

This threshold was set considering the distribution of the IQR picks, from selecting maximum IQR (IQR_{max}) by resampling data again using tri-hourly bins.

To compute the diurnal variation, we looked for what we refer as local quiet days (LQD) for each station. Basically, as done in [10], we consider as LQD, the five days with minor daily IQR picks. Then, we compute the average of the H component data during those five quietest days:

$$\langle LDQ_H(t) \rangle = \frac{1}{5} \sum_{i=1}^5 H_i(t) - \langle H_i[0 : 3](LT) \rangle \quad (7)$$

where we normalize the offset of each daily data by sustracting the average of the first 4 hours magnetic data in local time, as explained by the second term in the Equation 7. Hence we model the diurnal variation H_{SQ} from applying a low pass filter following the Equation (1) in [10] to the Fourier Transform of the result in Equation 7.

B MC Pherron Equation for Inyection function

$$\frac{dE(t)}{dt} = U(t) - \frac{E(t)}{\tau} \quad (8)$$

$$\frac{dDst^*}{dt} = Q(t) - \frac{Dst^*(t)}{\tau} \quad (9)$$

$$offset = Q\Delta t \quad (10)$$

$$Q(nT/h) = \begin{cases} a(E_Y - 0.5) & E_Y > 0.5mVm^{-1} \\ 0 & E_Y < 0.5mVm^{-1} \end{cases} \quad (11)$$

Acknowledgements Suspendisse vel felis. Ut lorem lorem, interdum eu, tincidunt sit amet, laoreet vitae, arcu. Aenean faucibus pede eu ante. Praesent enim elit, rutrum at, molestie non, nonummy vel, nisl. Ut lectus eros, malesuada sit amet, fermentum eu, sodales cursus, magna. Donec eu purus. Quisque vehicula, urna sed ultricies auctor, pede lorem egestas dui, et convallis elit erat sed nulla. Donec luctus. Curabitur et nunc. Aliquam dolor odio, commodo pretium, ultricies non, pharetra in, velit. Integer arcu est, nonummy in, fermentum faucibus, egestas vel, odio.

References

- [1] M. Blanc and A. D. Richmond. The ionospheric disturbance dynamo. *Journal of Geophysical Research*, 85(A4):1669–1686, April 1980. doi:10.1029/JA085iA04p01669.
- [2] C.I. Castellanos-Velazco, P. Corona-Romero, J.A. González-Esparza, M.A. Sergeeva, A.L. Caccavari-Garza, and V.J. Gatica-Acevedo. Low latitude geomagnetic response associated with intense geomagnetic storms: Regional space weather in mexico. *Journal of Atmospheric and Solar-Terrestrial Physics*, 259:106237, 2024. ISSN 1364-6826. doi:<https://doi.org/10.1016/j.jastp.2024.106237>. URL <https://www.sciencedirect.com/science/article/pii/S1364682624000658>.
- [3] G. R. J. Cooper and D. R. Cowan. Comparing time series using wavelet-based semblance analysis. *Computers and Geosciences*, 34(2):95–102, February 2008. doi:10.1016/j.cageo.2007.03.009.
- [4] J. W. Gjerloev. The SuperMAG data processing technique. *Journal of Geophysical Research (Space Physics)*, 117(A9):A09213, September 2012. doi:10.1029/2012JA017683.
- [5] INTERMAGNET. International real-time magnetic observatory network, 2021. URL <https://www.intermagnet.org/index-eng.php>.
- [6] D.J Knecht and . Shuman B.M. *HANDBOOK OF GEOPHYSICS AND THE SPACE ENVIRONMENT, chapter 4, THE GEOMAGNETIC FIELD*. ed by A. S. Jursa, Boston: Air Force Geophysics Laborator, 1985.
- [7] Atsuhiro Nishida. Geomagnetic D_p 2 fluctuations and associated magnetospheric phenomena. *Journal of Geophysical Research*, 73(5):1795–1803, March 1968. doi:10.1029/JA073i005p01795.
- [8] Henry Rishbeth and Owen K. Garriott. *Introduction to ionospheric physics*. 1969.
- [9] Christopher Torrence and Gilbert P. Compo. A practical guide to wavelet analysis. *Bulletin of the American Meteorological Society*, 79(1):61 – 78, 1998. doi:10.1175/1520-0477(1998)079<0061:APGTWA>2.0.CO;2. URL https://journals.ametsoc.org/view/journals/bams/79/1/1520-0477_1998_079_0061_apgtwa_2_0_co_2.xml.
- [10] M. van de Kamp. Harmonic quiet-day curves as magnetometer baselines for ionospheric current analyses. *Geoscientific Instrumentation, Methods and Data Systems*, 2(2):289–304, November 2013. doi:10.5194/gi-2-289-2013.
- [11] W. Younas, C. Amory-Mazaudier, Majid Khan, and R. Fleury. Ionospheric and Magnetic Signatures of a Space Weather Event on 25-29 August 2018: CME and HSSWs. *Journal of Geophysical Research (Space Physics)*, 125(8):e27981, August 2020. doi:10.1029/2020JA027981.
- [12] Waqar Younas, C. Amory-Mazaudier, Majid Khan, and M. Le Huy. Magnetic Signatures of Ionospheric Disturbance Dynamo for CME and HSSWs Generated Storms. *Space Weather*, 19(9):e02825, September 2021. doi:10.1029/2021SW002825.